ARCHIVES
of
FOUNDRY ENGINEERING

ISSN (2299-2944)
Volume 2026
Issue 1/2026

52 – 67

10.24425/afe.2026.157969

6/1

Published quarterly as the organ of the Foundry Commission of the Polish Academy of Sciences

AlSiMg Alloys Microstructure Determined by Flow Effect During Slow Solidification

P. Mikolajczak
Poznan University of Technology, Poland
Correspondence contact: E-mail address: Piotr.Mikolajczak@put.poznan.pl

Received 05.05.2025; accepted in revised form 19.06.2025; available online 09.03.2026

Abstract

The presence of gravity during pouring, causes the flow of the alloy in the gating system and the mold cavity, as well as the phenomenon of natural convection at the stage of solidification of the casting. However, the developed casting technologies also use the phenomenon of forced convection, which can be generated by mechanical or electromagnetic mixers. The effect of stirring with electromagnetic coils on the microstructure of Al-Si-Mg alloys was analyzed, based on slowly solidifying small cylindrical samples. In tested Al-Si-Mg alloys, melt flow led to microstructure modification: changed amount, dimension, and location of magnesium-rich Mg_2Si precipitates, secondary dendrite arm spacing SDAS, specific surface and grain size of α-Al phase and finally modified eutectic spacing for observed binary and ternary eutectics. Flow produced more and larger blocky shaped and Chinese script phases and significantly reduced amount and dimension of dispersed Mg_2Si in the alloy where Mg_2Si grow as first phase. By co-precipitation of α-Al and Mg_2Si with a basically dendritic shape and internal form of Mg_2Si, forced flow increased its SDAS, produced globular forms, whilst did not change the internal spacing. In the alloy where α-Al and Si crystals co-precipitate, stirring caused formation of characteristic eutectic-enriched regions separated from α-Al rich regions. In the alloy where Mg_2Si and Si co-precipitate before eutectic growth, stirring caused distinct appearance of dendritic Mg_2Si and α-Al. The observed structural modifications are new and can help in assessing of convection effect on microstructure of industrial alloys and support the design of casting processes in which mechanical or electromagnetic stirring is the main phenomena determining microstructure and mechanical properties of cast parts.

Keywords: Casting structure, Aluminum alloys, Convection, Solidification, Mg_2Si phases, α-Al phase

1. Introduction

Aluminum alloys are commonly used e.g. in the automotive, aeronautics and others for the production of many different parts. Excellent castability of Al-Si-Mg cast alloys enable production of complex-shape components with high specific strength. The more requirements concerning performance enhancement or fuel emissions reductions are leading towards design and manufacturing concepts, which induce higher mechanical and thermal loads on machines elements [1,2]. To the Al-Si alloys, for e.g. thermal stability copper (Cu) is added, whilst for more hardness iron (Fe) is added. Also Mn, Mg, Zn and other elements are present in Al-Si alloys, where between primary dendritic grains of α-Al with Al-Si eutectics some other phases form, e.g. Mg_2Si.

In the aluminum alloys containing Si and Mg, intermetallic compound Mg_2Si is a key phase, because it exhibits low coefficient of thermal expansion (7.5×10^{-6} K^{-1}), high elastic modulus (120 GPa), high melting temperature (1085 ˚C), low density (1.99×10^3 kgm^{-3}) and high hardness (4500 MNm-2), [3,4]. Mg_2Si forms into Chinese script eutectics and coarse dendritic primary phase, and these shapes significantly reduce mechanical properties, because tips of eutectic Mg_2Si and edges occurring by coarse dendritic Mg_2Si become stress concentration points [5].

In order to improve mechanical properties trough controlling size, morphology and distribution of Mg_2Si, previous studies were focused on the addition of nucleants such as Li [6], Na [7,8], Ni [9], P [10,11], Sr [10,12], AlP [13,14], TiB2 [14] and by use of heat treatment [6], however, an alternative simple cheap and efficient method is still being sought.

Technologies are being developed in foundry: high shear conditioning (HSMC) [15], mechanical stirring [16], melt conditioning (MC) [17], semisolid processing (SSM) [18], rheocasting [19,20], thixoforming [21,22] or electromagnetic stirring (EMS) [23,24] by inducing rotating magnetic fields (RMF). Improved mechanical properties of Al based alloys [25] and composites [26] or special rheological properties [27] result from a non-dendritic structure [28].

Application of mechanical or electromagnetic stirring of Al-Si alloys by the presence of Mg_2Si phases require studying physical processes, microstructure growth and transformation occurring by forced flow.

In the current study, Al-Si-Mg alloys were prepared from high purity components in order to simplify the microstructures studied. The Al-Si-Mg alloys compositions, based on the phase diagram (Fig. 1), were selected in order to conduct in common (joint growth) or independent (separate) growth of occurring phases: Mg_2Si intermetallics, Al-Si eutectics, Si crystals and α-Al phases. During such introduced precipitation conditions, the effect of natural or forced convection was investigated: a) on selected and growing individually phases or on b) phases growing together.

The main motivation was to study the effect of rotating magnetic field (RMF) and occurring melt flow on the microstructure and individual phases in Al-Si-Mg alloys, in aspect of casting technologies development, e.g. [15-17, 19-21, 23-28].

2. Materials and methods

To study separate or joint growth of occurring phases, alloys from Al-Si-Mg phase diagram (Fig. 1) were selected.

Defined in current study independent growth means precipitation of only one phase, starting at liquidus temperature and lasting till eutectic reaction. The joint growth was defined as co-precipitation of two phases, starting at liquidus temperature and following e.g. monovariant line on phase diagram and finally finishing of course at solidus with growth of remaining phases, e.g. AlSi eutectics. In this Al-Si-Mg system, the solidus temperature is 558.65 ˚C, whilst 585.00 ˚C as liquidus temperature was chosen determining in this way alloys compositions. For separate (independent) precipitation were selected three alloys:

- "α-Al-first" alloy (Figure 1, blue solid line) - composition AlSi9.430Mg3.470, from the melt, α-Al phase precipitates first at 585 ˚C till 558.67 ˚C,
- "Mg_2Si-first" alloy (Figure 1, red solid line) - composition AlSi13.070Mg5.845, from the melt, Mg_2Si phase precipitates first at 585 ˚C till 558.67 ˚C,
- "Si-first" alloy (Figure 1, green solid line) - composition AlSi14.180Mg4.400, from the melt, Si crystals precipitate first at 585 ˚C till 558.67 ˚C,

For (common) co-precipitation were selected three alloys too:

- "α-Al/Mg_2Si" alloy (Figure 1, violet dashed line) - composition AlSi6.470Mg7.840, from the melt α-Al phase co-precipitate with Mg_2Si starting both at 585 ˚C,
- "α-Al/Si" alloy (Figure 1, yellow dashed line) - composition AlSi12.515Mg2.250, from the melt α-Al phase with Si crystals co-precipitate starting both at 568 ˚C, this liquidus temperature differs from other alloys and results from chosen middle of the monovariant (red) line on the phase diagram,
- "Mg_2Si/Si" alloy (Figure 1, grey dashed line) - composition AlSi14.510Mg5.630, from the melt, Mg_2Si with Si crystals co-precipitate starting both at 585 ˚C.

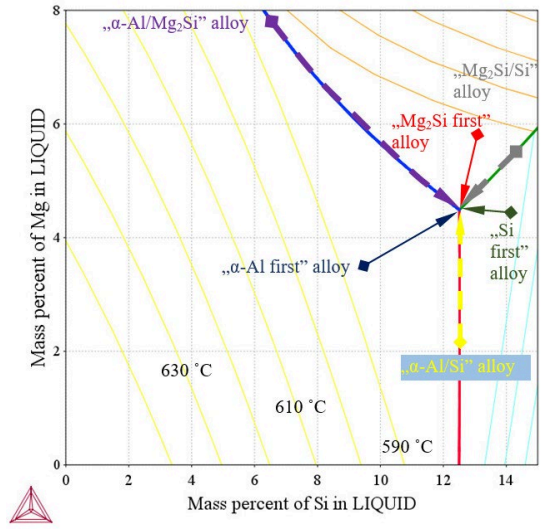

Fig. 1. Ternary Al-Si-Mg phase diagram with for studied alloys marked solidification paths, e.g. dashed gray line for Mg_2Si/Si (AlSi14.510Mg5.630) alloy

Solidification of alloys was conducted in the device [29] owing set of coils powered from network via an autotransformer (Tufvassons, Sigtuna, type KIEA 4). The facility was specially designed in order to study flow effect on the microstructure and previously applied [30-34] for Al alloys. The APAR AR 207 data recorder with thermocouples type K (TP-203) was applied in order to control thermal conditions. The coils generating rotating magnetic field (RMF) [29] were located near to the casting and the graphite crucible, and protected using copper cooler and insulation with conductivity of about 0.1 W/mK (Fiberfrax, USA). Such a construction allowed slow solidification by low temperature gradient about 0.143 K/mm and low cooling rate about 0.112 K/s [29].

The alloys were prepared from high purity materials, Mn (99.98%), Si (99.9999%) and Al (99.999%) melted 1.5 h at 800 ˚C in electric resistance by constant flush of argon (more details in [29-34]). Next graphite crucible with alloy was quickly moved together into the facility where specimens slowly solidified by natural (0 mT) or forced convection (with 11 mT RMF).

Similarly to [29-34], cut microsections (Fig. 2a) were prepared with standard metallographic procedure and investigated with a microscope (MA200 Nikon, Japan) by magnifications from

50× till 500×. On the polished sections, occurring in the microstructure phases were observed and measured in small areas A, B and C (Fig. 2c, white filled rectangles) or in larger one (white dashed line rectangle).

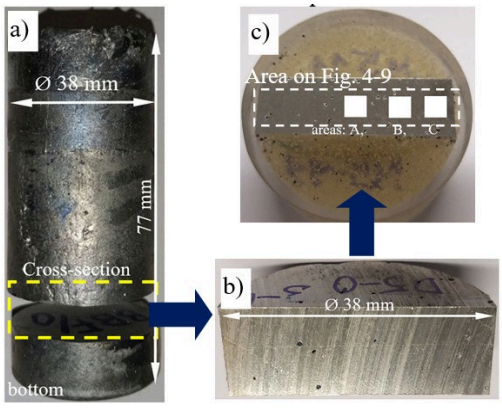

Fig. 2. Processed specimens: a) place for cutting the cross-section, b) cut out sample with the section along the sample axis, c) filled rectangle areas A, B and C for parameters measurement and dashed line rectangle showing area presented on Fig. 4-9

The following parameters were determined in mentioned specimen regions and calculated as the average value for the whole sample: number density n_{blocky}, $n_{dispersed}$, $n_{Chinese}$ and average diameter L_{blocky}, $L_{dispersed}$, $L_{Chinese}$ of magnesium-rich Mg_2Si precipitates (blocky, dispersed or Chinese script shaped), spacing λ_X, $\lambda_{X\text{-}Mg2Si}$, $\lambda_{X\text{-}Al\text{-}Mg2Si}$ observed in Mg_2Si phases (Fig. 3), secondary dendrite arm spacing (SDAS) $\lambda_{SDAS}=\lambda_2$, average grain size L_{Al} and average specific surface S_v of α-Al, and finally average spacings λ_{AlSi}, $\lambda_{Al\text{-}Mg2Si}$ and $\lambda_{Ternary}$ for observed binary and ternary eutectics.

The averaging of the distance between adjacent plates was applied in order to calculate eutectic spacing λ_{AlSi}, $\lambda_{Al\text{-}Mg2Si}$ and $\lambda_{Ternary}$. Similarly and as presented on Fig. 3, spacings λ_X, $\lambda_{X\text{-}Mg2Si}$, $\lambda_{X\text{-}Al\text{-}Mg2Si}$ were determined. The averaging of the distance between 15-45 adjacent side branches for determination of SDAS λ_2 was applied. The specific surface S_v of α-Al, as the ratio of the perimeter and the enclosed area was calculated. The spacing λ_X (Fig. 3) for Mg_2Si was considered similarly to SDAS, as the average distance between branches of formed Mg_2Si phases.

The occurred in microstructures phases are well-known to the author from previous investigations [30] and many other studies [3-14]. The methodology was previously developed and perfected in [29-34]. The alloys were first chosen according to phase diagram (Fig. 1), than exactly determined in numerical thermodynamic calculations with Thermocalc [35] concerning Scheil solidification calculation, property diagrams and the ternary phase diagram.

The thermodynamic calculations [35] helped to determine solid mass fraction of occurring phases at specified temperatures and exact Al-Si-Mg alloys compositions, by that only one and first phase grow (e.g. Mg_2Si in the "Mg_2Si-first" alloy) or precipitate both jointly (e.g. Mg_2Si and Si in "Mg_2Si/Si" alloy).

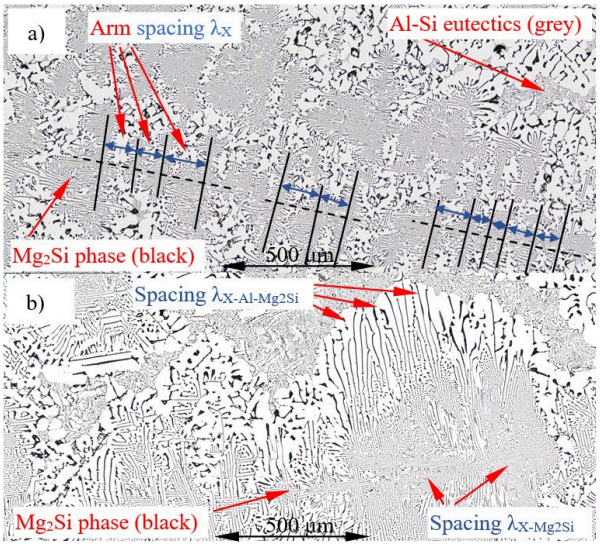

Fig. 3. Methodology of the parameters measurement for Mg_2Si phases. Microstructures of the α-Al/Mg_2Si (AlSi6.470Mg7.840) alloy solidified by: a) only natural convection 0 mT and (b) electromagnetic field 11 mT. Dashed black lines mark primary arm and continues black lines mark secondary arm of similar to dendrite structures

3. Results

This chapter presents stirring effect on: the microstructure along the whole specimens diameter and in more detail on specified places, parameters characterizing size or number density of formed phases, and the order in growth of occurring phases.

3.1. Microstructure

Fig. 4 presents microstructures of α-Al first alloy specimens (AlSi9.430Mg3.470) solidified with and without melt flow, with clearly visible α-Al dendrites uniformly distributed across both specimens. By forced convection (RMF 11 mT) dendritical forms seems to be shorter (Fig. 4b) and there is lack of long primary arms of dendrites as seen (Fig. 4a) by natural convection (0 mT).

Microstructures (Fig. 5) of Mg_2Si first alloy specimens (AlSi13.070Mg5.845) solidified without and with forced flow shows both similar and very uniform distribution of small phases. By electromagnetic stirring, it seems to be formed some very small and rarely occurring dendrites.

On the Fig. 6 of Si first alloy (AlSi14.180Mg4.400) specimens, AlSi eutectics occupies most of the area, with the minority presence of α-Al dendrites uniformly distributed across both specimens, by 0 and 11 mT.

Microstructures (Fig. 7) of the α-Al/Mg_2Si alloy specimens (AlSi6.470Mg7.840) seems to be very similar with uniformly distributed principates, and they do not reveal any effect of electromagnetic melt stirring.

Fig. 8 presents microstructures of α-Al/Si alloy specimens (AlSi12.515Mg2.250) solidified with and without melt flow, with

clearly visible α-Al dendrites more or less uniformly distributed across both specimens, and AlSi eutectics filled the space between dendrites. By forced convection (RMF 11 mT) dendritical forms seems to be shorter (Fig. 8b) and some areas without dendrites and rich in AlSi eutectics occurred.

On the microstructures of the Mg_2Si/Si (AlSi14.510Mg5.630) alloy specimen mostly AlSi eutectic occurs with some dendritical forms. Solidified by forced flow (Fig. 9b) microstructure presents less uniformly distributed small α-Al dendrites and perhaps more AlSi eutectics.

More microstructure details of tested alloys is visible by higher magnification (100× till 500×). Forced flow caused clearly visible on Fig. 10b smaller α-Al dendrites with occurring globular α-Al forms in α-Al first alloy. In the Mg_2Si first alloy (Fig. 11a) precipitated small dispersed Mg_2Si (black color) and some large blocky shaped Mg_2Si (Fig. 12), surrounded by α-Al phase (white) and AlSi eutectics (grey), but forced flow (Fig. 11b) caused formation of well visible AlSi eutectics with small α-Al dendrites, Chinese script shaped Mg_2Si and almost lack of dispersed Mg_2Si. As seen on Fig. 13, microstructures of the Si first alloy presents similarly with lot AlSi eutectic and in minority α-Al forms. In the α-Al/Mg_2Si alloy specimen, Mg_2Si phase formed according to dendritical scheme (Fig. 14a), which was modified by forced flow into smaller globular forms (Fig. 14b). On the Fig. 15b for α-Al/Si alloy solidified by stirring, very well visible is area rich in the AlSi-eutectics clearly separated from area rich in globular and dendritical α-Al phase, in opposite to natural convection where even distribution may be observed. In the Mg_2Si/Si alloys specimen (Fig 16) was AlSi eutectics with some small dendrites observed, by the presence of blocky shaped Mg_2Si (Fig. 17) and larger spreading Mg_2Si phases (Fig. 18). In this alloys flow caused formation of dendritic Mg_2Si on the outer specimen surface (Fig. 19 as a detail from Fig. 16) similarly with rich in Al globular and dendritic forms (Fig. 20 as a detail from Fig. 16).

3.2. Parameters characterising microstructure

The influence of forced convection induced by electric coils was assessed on the basis of parameters characterizing the resulting phases in the observed microstructures. Large number of considered precipitates, crystals, grains or dendrites arms ensured high accuracy and high quality of results.

In Tables 1-4, values of different parameters are given, whilst in square brackets standard deviation. In parentheses the studied parameters variation resulting from induced by electric coils forced flow is presented and in curly brackets solidification time.

Forced flow increased by 17% (Tab. 1) secondary dendrite arm spacing SDAS λ_{SDAS}, from 54.8 to 68.3 μm, by standard deviation 4.4 and 3.9 μm in α-Al first alloy, where the majority of them is α-Al phase. By stirring induced growth of SDAS was also observed in Si first alloy (+6%) and α-Al/Si alloy (+5%), whilst a decrease in Mg_2Si/Si alloy was observed. In all alloys where α-Al occurred, flow decreased significantly the average grain size L_{Al} (Tab. 1), 66% for α-Al first alloy, 42% for Si first alloy, 60% α-Al/Si alloy and 28% for Mg_2Si/Si alloy. Average specific surface S_V of α-Al phase decreased 31% and 29% in α-Al first alloy and α-Al/Si alloy respectively, also in the alloys where this phase is quite good present. By stirring, S_V increased 24% and 8% in Si first alloy and Mg_2Si/Si alloy respectively.

The eutectic spacings λ_{AlSi} , $\lambda_{Al\text{-}Mg2Si}$ and $\lambda_{Ternary}$ (Table 1), both decreased or increased for individual alloys, and the effect of by coil induced stirring on eutectic phases seems unclear. For the α-Al first alloy, the eutectic spacing λ_{AlSi} decreased by 36% from 11.64 μm to 7.44 μm, with standard deviation values of 0.649 μm and 0.974 μm, whilst for α-Al/Si alloy changed only 2%. The eutectic spacing $\lambda_{Al\text{-}Mg2Si}$ for the α-Al first alloy, remained almost unchanged (1% modification), whilst for Si first alloy decreased by 14% from 7.45 to 6.42 μm. The ternary eutectic spacing $\lambda_{Ternary}$, influenced by stirring, for the α-Al first alloy increased significantly 62%, from 3.29 to 5.33 μm, whilst for other alloys decreased, e.g. 52%, from 11.13 to 5.39 for Mg_2Si first alloy. Generally, the changes amount from -42% to 31% for eutectic spacing λ_{AlSi} , -52% to 62% for ternary eutectic spacing $\lambda_{Ternary}$, whilst eutectic spacing $\lambda_{Al\text{-}Mg2Si}$ seems to be more stable, with changes from -14% to 13%.

Observed in α-Al/Mg_2Si alloy (Fig. 14) characteristically formed Mg_2Si precipitate was measured according to methodology presented on Fig. 3, and forced flow effect by changes -2% and -2% (Tab. 2) for $\lambda_{X\text{-}Mg2Si}$ and $\lambda_{X\text{-}Al\text{-}Mg2Si}$ is negligible. The spacing λ_X , similar to secondary dendrite arms spacing of α-Al phase, increased 10% under forced flow. The values of λ_X (62.73 and 69.35 μm) seems to be similar to secondary dendrite arm spacing λ_{SDAS} (54.8 and 68.3 μm) of α-Al phase in α-Al first alloy.

Occurring in Mg_2Si first alloy (Fig. 11 and 12) Mg_2Si phase forms as small dispersed, Chinese script and some large blocky shaped precipitates. Forced flow increased by 41% average overall dimension L_{blocky} (Tab. 3, from 91.1 to 128.9 μm) of blocky shaped Mg_2Si, and increased by 118% its number density n_{blocky} (Tab. 4, from 2.093 to 4.567 mm^{-2}). Similarly, stirring increased by 116% and by 336%, average overall dimension $L_{Chinese}$ (Tab. 3) and number density $n_{Chinese}$ (Tab. 4) of Chinese script shaped Mg_2Si, respectively. The opposite situation occurred for small dispersed Mg_2Si precipitates, where forced convection decreased by 65% and by 98%, average overall dimension $L_{dispersed}$ and number density $n_{dispersed}$.

3.3. Precipitation sequence

The assumptions of the adopted methodology were fulfilled based on thermodynamic calculations [35], where composition precisely was determined, together with characteristic temperatures, precipitation sequence, and mass fraction of precipitating phases (Tab. 5).

Based on the ternary Al-Si-Mg phase diagram (Figure 1), by assumed liquidus temperature 585 ˚C (for almost all studied alloys), the initial composition AlSi9.5Mg3.5 was proposed for the alloy, where *α*-Al should be the first and initially only one growing phase. Next, Scheil solidification and property diagram resulting from iterative thermodynamic calculations and carried out analysis, provided resulting exact AlSi9.430Mg3.470 alloys composition. In this "*α*-Al first" alloy (Tab. 5), starting from

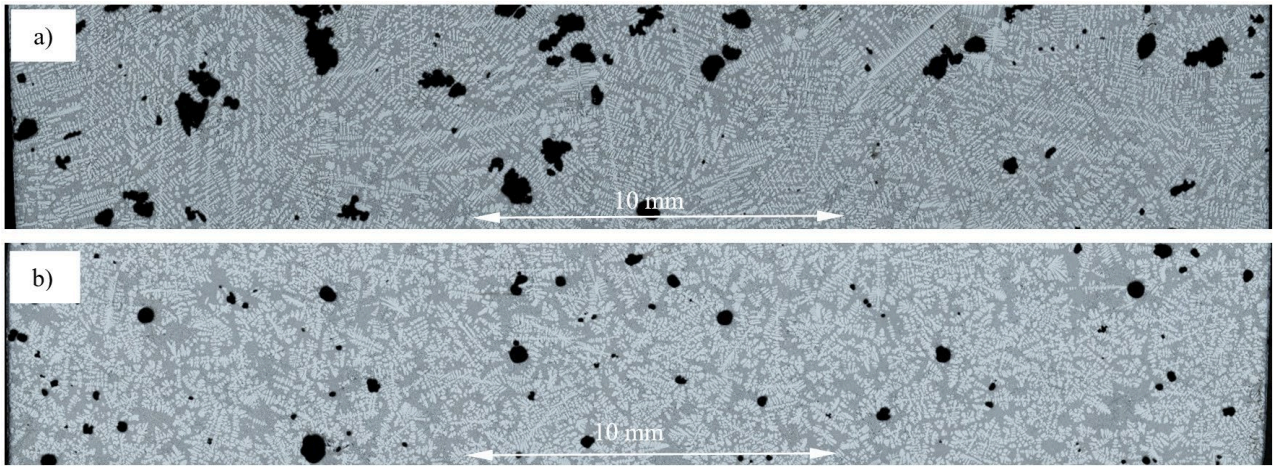

Fig. 4. Microstructures of the α-Al first (AlSi9.430Mg3.470) alloy specimen solidified by: a) only natural convection 0 mT and (b) electromagnetic field 11 mT

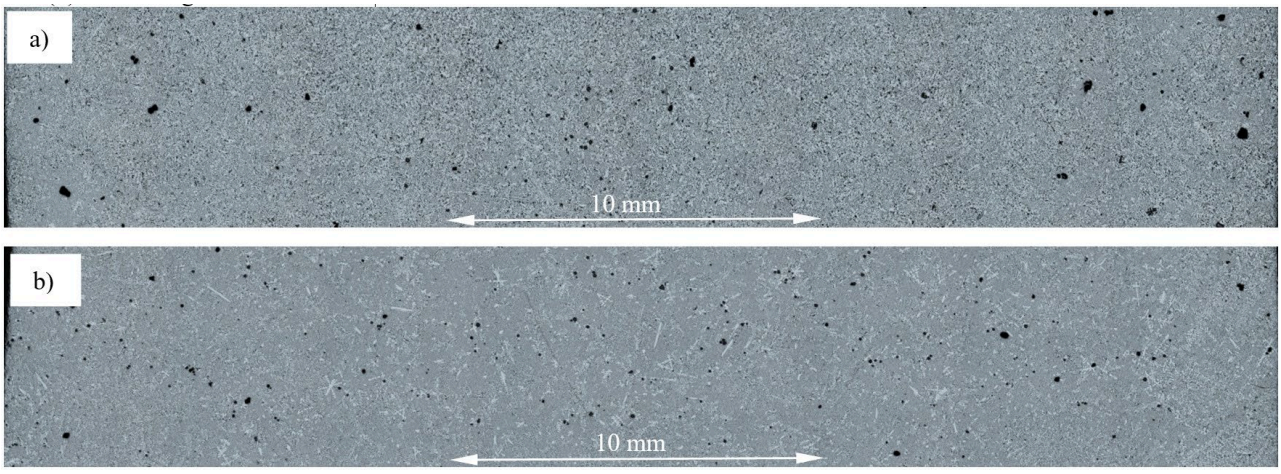

Fig. 5. Microstructures of the Mg_2Si first (AlSi13.070Mg5.845) alloy specimen solidified by: a) only natural convection 0 mT and (b) electromagnetic field 11 mT

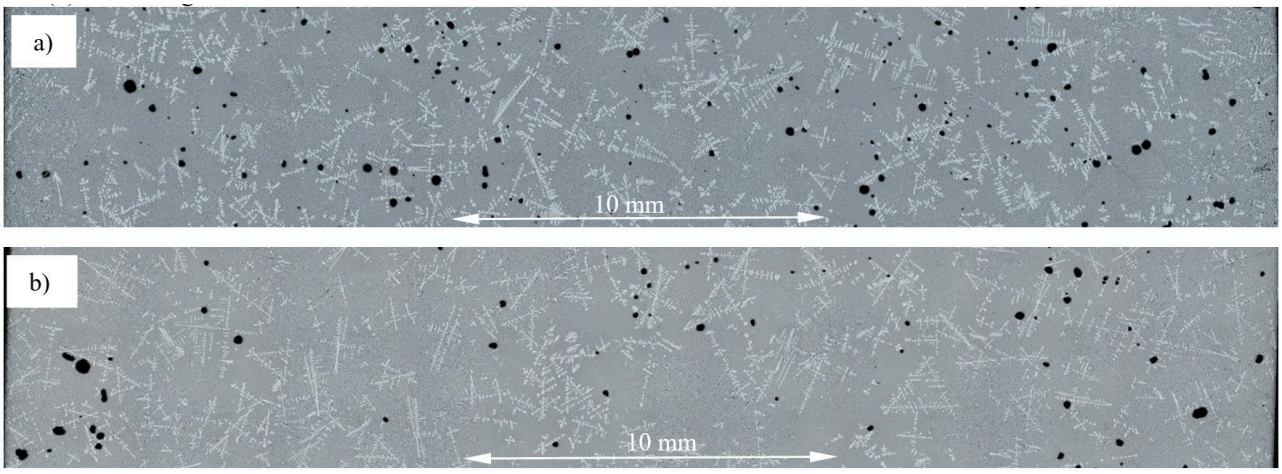

Fig. 6. Microstructures of the Si first (AlSi14.180Mg4.400) alloy specimen solidified by: a) only natural convection 0 mT and (b) electromagnetic field 11 mT

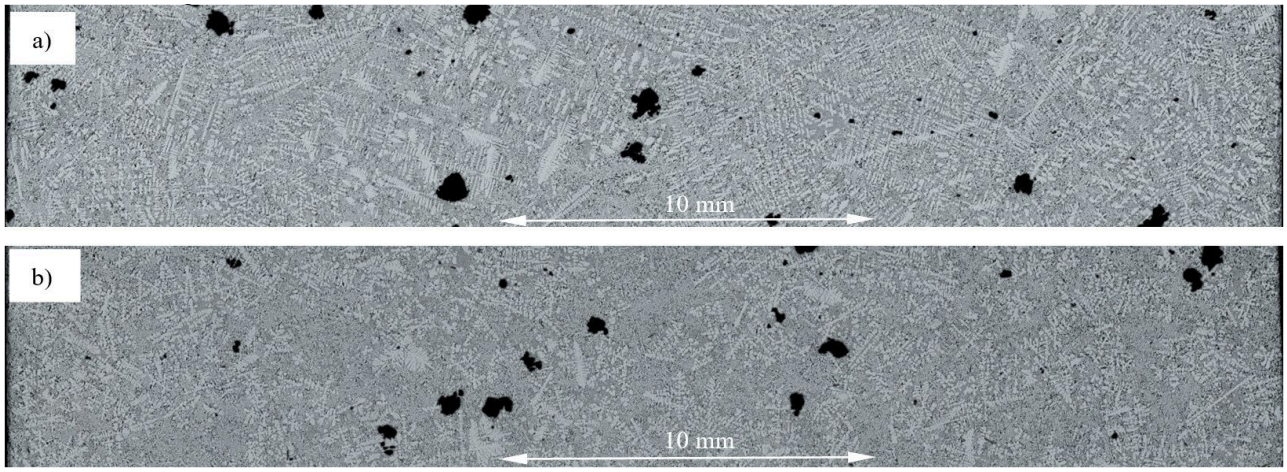

Fig. 7. Microstructures of the α-Al/Mg_2Si (AlSi6.470Mg7.840) alloy specimen solidified by: a) only natural convection 0 mT and (b) electromagnetic field 11 mT

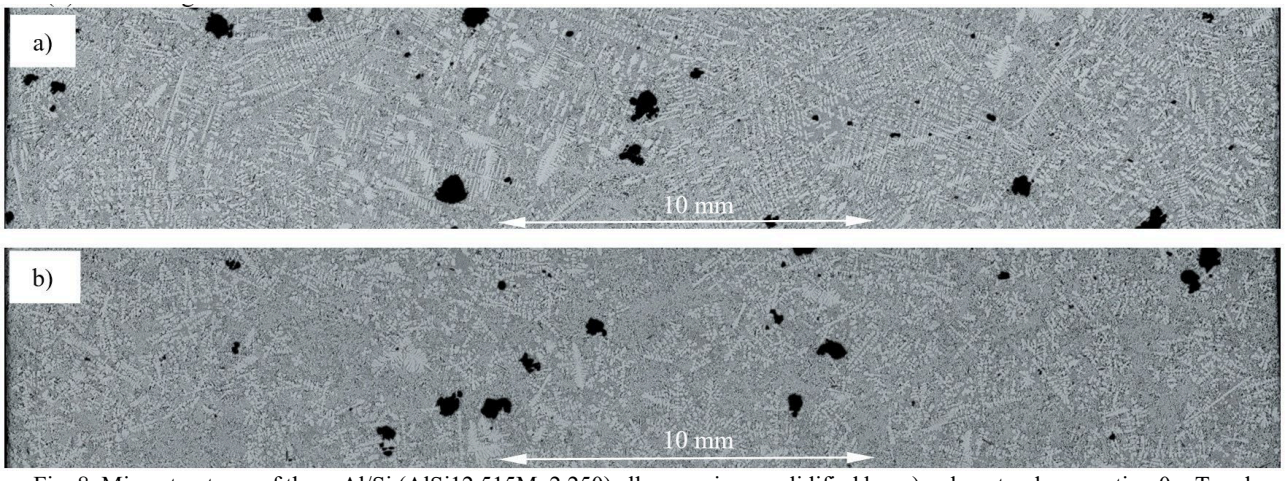

Fig. 8. Microstructures of the α-Al/Si (AlSi12.515Mg2.250) alloy specimen solidified by: a) only natural convection 0 mT and (b) electromagnetic field 11 mT

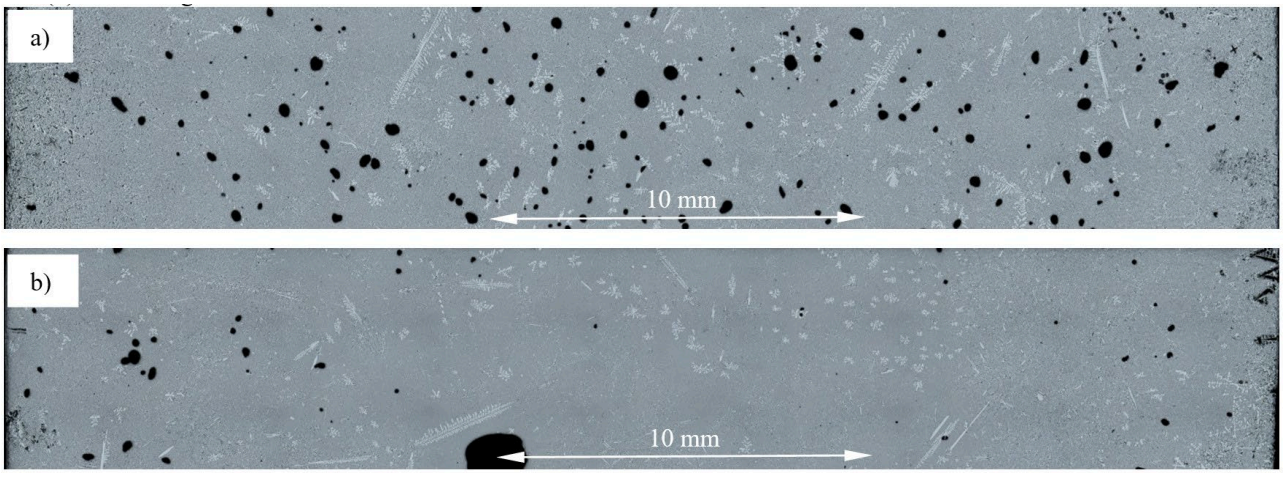

Fig. 9. Microstructures of the Mg_2Si/Si (AlSi14.510Mg5.630) alloy specimen solidified by: a) only natural convection 0 mT and (b) electromagnetic field 11 mT

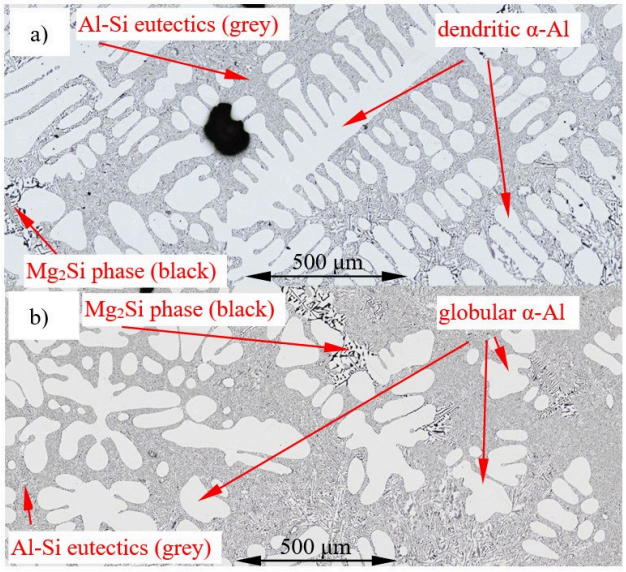

Fig. 10. Microstructures of the α-Al first (AlSi9.430Mg3.470) alloy specimen solidified by: a) only natural convection 0 mT and (b) electromagnetic field 11 mT

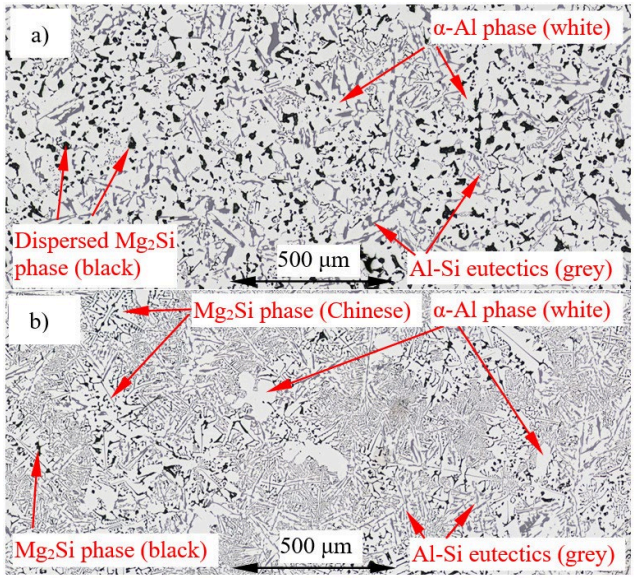

Fig. 11. Microstructures of the Mg_2Si first (AlSi13.070Mg5.845) alloy specimen solidified by: a) only natural convection 0 mT and (b) electromagnetic field 11 mT

liquidus temperature 585 ˚C and according to reaction described as L → α-Al + L, *α*-Al phase will grow. Similarly with growth and cooling, the melt enriches in Mg and Si and finally reaches temperature 558.67 ˚C. At this temperature 558.67 °C till 558.65, occurred L → α-Al + Mg_2Si + Si as the final eutectic reaction, where mass fraction of *α*-Al reaches $f_{\alpha\text{-Al}}$ = 89.03%, Mg_2Si mass fraction f_{Mg2Si} = 4.33%, and eutectics mass fraction reaches f_{Eut} = 6.64%.

Similarly chemical compositions, occurring reactions and mass fraction of phases for other alloys were determined (Tab. 5) and it is clear that the main idea of current study was practically fulfilled.

From the Table 5, it can be concluded that studied alloys form two groups, one where till start of final eutectic reaction at 558.67 ˚C, only 2.30% (Mg_2Si first alloy), 1.90% (Si first alloy) and 2.07% (Mg_2Si/Si alloy) of solid mass fraction precipitated, in opposite to 72.38% (α-Al first alloy), 87.28% (α-Al/Mg_2Si alloy) and 59.47% (α-Al/Si alloy) of solid mass fraction.

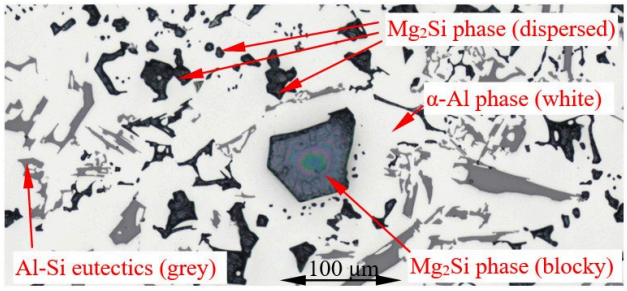

Fig. 12. Microstructure of the Mg_2Si first (AlSi13.070Mg5.845) alloy specimen solidified by only natural convection 0 mT

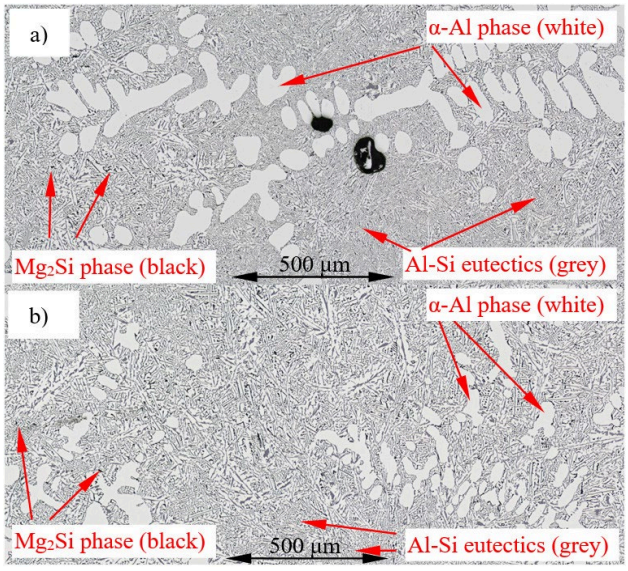

Fig. 13. Microstructures of the Si first (AlSi14.180Mg4.400) alloy specimen solidified by: a) only natural convection 0 mT and (b) electromagnetic field 11 mT

4. Discussion

Based on the collected results, it is possible to discuss the impact of forced convection on selected Al-Si-Mg alloys. The basis of the analysis are microstructures and measured parameters characterizing the distribution, size, shape and number density of phases released such as *α*-Al phase, Mg_2Si and eutectics.

4.1. α-Al crystals

In the α-Al first alloy according to phase diagram and with authors intention α-Al phase formed correctly (Fig. 4 and 10), and similarly in α-Al/Si alloy (Fig. 8 and Fig. 15). In other alloys not any dendritical α-Al phase should form, but as effect of some thermal and composition fluctuation, α-Al may be on Fig. 5b, 6, 9, 11b, 13 and 16 observed.

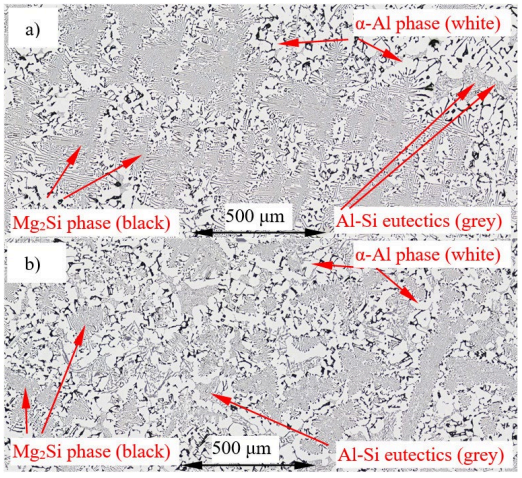

Fig. 14. Microstructures of the α-Al/Mg_2Si (AlSi6.470Mg7.840) alloy specimen solidified by: a) only natural convection 0 mT and (b) electromagnetic field 11 mT

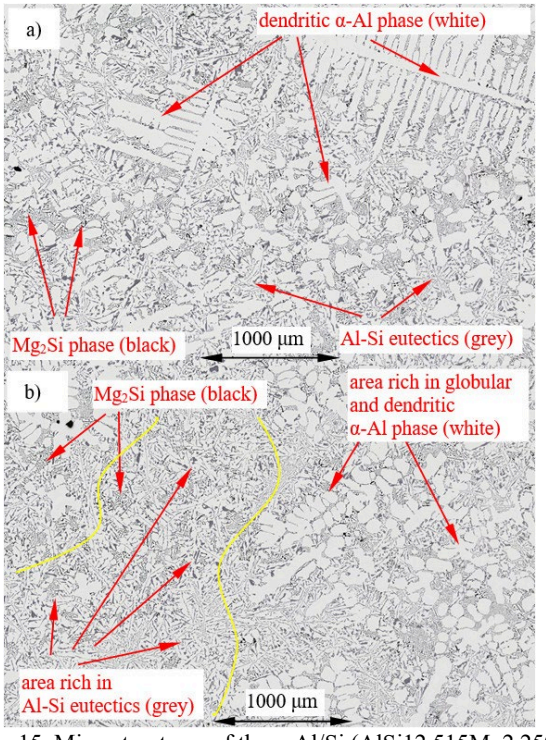

Fig. 15. Microstructures of the α-Al/Si (AlSi12.515Mg2.250) alloy specimen solidified by: a) only natural convection 0 mT and (b) electromagnetic field 11 mT

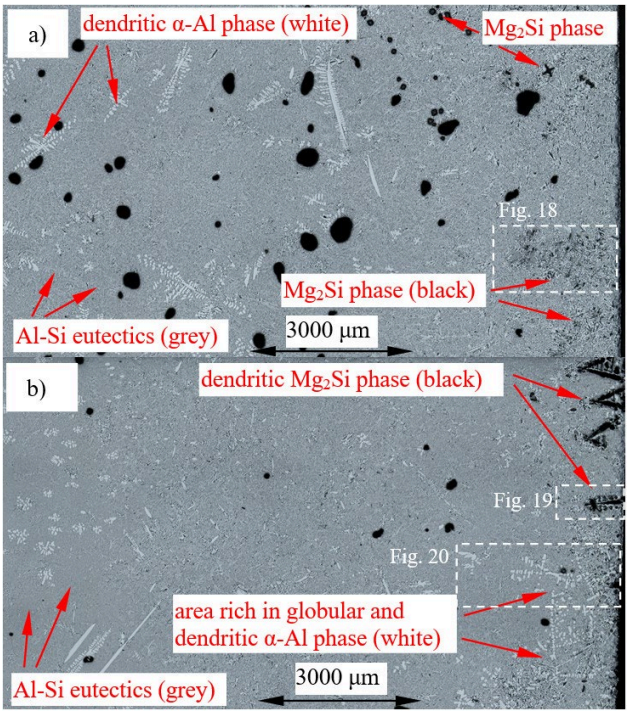

Fig. 16. Microstructures of the Mg_2Si/Si (AlSi14.510Mg5.630) alloy specimen solidified by: a) only natural convection 0 mT and (b) electromagnetic field 11 mT

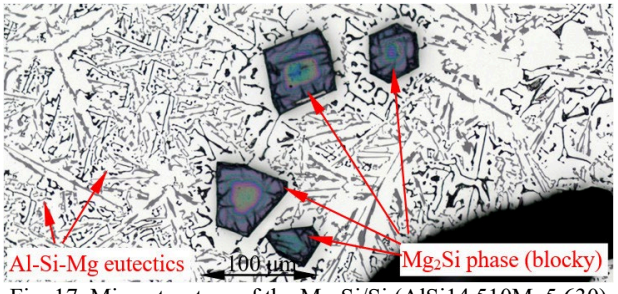

Fig. 17. Microstructure of the Mg_2Si/Si (AlSi14.510Mg5.630) alloy specimen solidified by only natural convection 0 mT

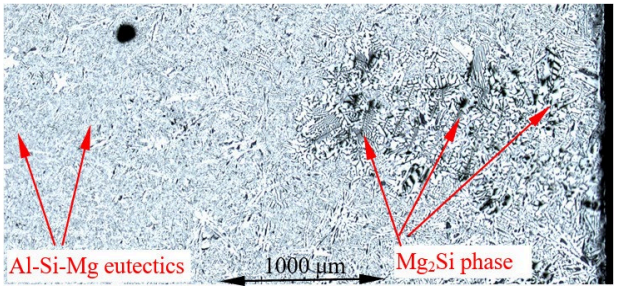

Fig. 18. Microstructure of the Mg_2Si/Si (AlSi14.510Mg5.630) alloy specimen solidified by only natural convection 0 mT

Flemings and Martinez presented [36] that intensive melt stirring may in mushy zone cause microstructure formation with spheroids. Also many other researchers studied phenomena of

structure modification by forced convection, e.g. Mullis in mathematical modelling and numerical simulations [37], Li on (SCN)-5% water succinonitrile [38] and classically on AlCu alloys Niroumand [39], Birol [40] and Fan [41].

For equiaxed dendrites formed by low temperature gradient and low cooling rate, the structure is frequently described by secondary dendrite arm spacing $\lambda_2=\lambda_{SDAS}$, and by slow solidification and diffusion-controlled growth, the value of Secondary Dendrite Arm Spacing SDAS may be calculated based [42] on:

$$\lambda_2 = c_1 \cdot t^{n1} \tag{1}$$

where, as (1) defined for the diffusive only mass transport n_1 amounts 0.33 and c_1 is materials depending coefficient [42]. For convective regime in directional solidification of AlSi-base alloys Steinbach and Ratke [43] designated $n_1 = 0.48$.

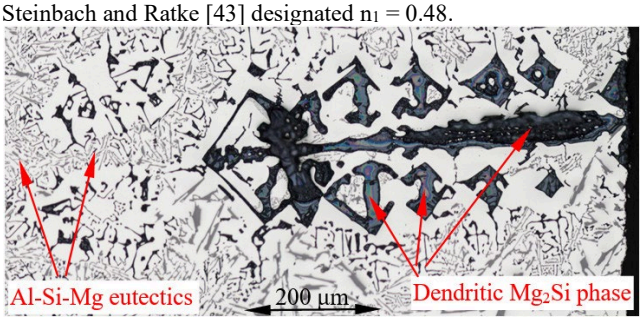

Fig. 19. Microstructure of the Mg_2Si/Si (AlSi14.510Mg5.630) alloy specimen solidified by electromagnetic field 11 mT

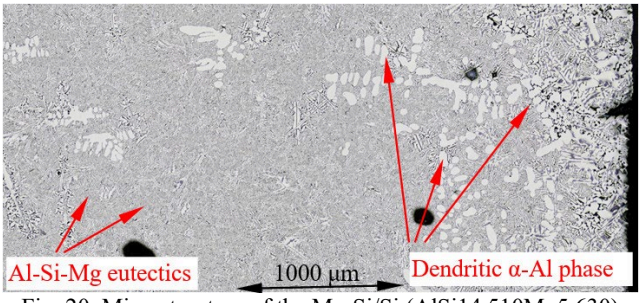

Fig. 20. Microstructure of the Mg_2Si/Si (AlSi14.510Mg5.630) alloy specimen solidified by electromagnetic field 11 mT

For the α-Al first alloy (Tab. 1), the electromagnetic stirring increased secondary dendrite arm spacing λ_2 by 17%, from 54.8 to 68.3 μm and by standard deviation of σ=4.4 and 3.9 μm. For the α-Al/Si and Si first alloy (Tab. 1) the forced flow caused an approximate 5% and 6% changes in λ_2, from 67.7 to 71.0 μm and from 41.4 to 43.8 μm respectively, and by calculated standard deviations σ=5.7 μm, 2.6 μm, 8.3 μm and 2.2 μm, the SDAS modifications appear small. For the Mg_2Si/Si alloy (Tab. 1), melt stirring decreased λ_2 by 10%, from 38.7 to 34.8 μm, by standard deviation of σ=2.9 and 1.9 μm.

Based on the measured solidification time (Tab. 1), measured secondary spacing λ_2 and equation (1), to obtain compliance of the measurement results with those calculated, the values of the material coefficient c_1 were determined for natural convection, and amounts 5.9, 4.8, 6.6 and 4.8 for α-Al first, Si first, α-Al/Si and Mg_2Si/Si alloys respectively, by $n_1 = 0.33$. For the case of melt stirring, the coincidence between measured and calculated λ_2 needs modification in the value of n_1, that as found in the literature [43] for directional solidification of AlSi-base alloys, should amount $n_1 = 0.47$-0.50. In the current study, consistency of results was obtained with exponent n_1 values of 0.38, 0.355, 0.35, and 0.30 for α-Al first, Si first, α-Al/Si and Mg_2Si/Si alloys respectively, and this is much smaller than 0.47-0.50 [43]. For similar solidification conditions, by low temperature gradient and low cooling rate, and Al-Si-Mn alloys closer n_1 values to currently calculated were found. For the AlSi7.887Mn0.379 alloy [33], similar to α-Al first (AlSi9.430Mg3.470) alloy where the α-Al precipitate grows as first, n_1 amounts 0.3365. For the similar to current α-Al/Si (AlSi12.515Mg2.250) studied in [33] AlSi12.536Mn0.296 alloy, n_1 amounts exactly the same 0.35. For the similar to current Si first alloy (AlSi14.180Mg4.400) studied in [34] AlSi14.732Mn0.567 alloy, n_1 amounts the same 0.376, that is slightly higher than currently determined 0.355. For the studied in [34] Mn/Si alloy (AlSi14.870Mn1.159), that could be similar to currently investigated Mg_2Si/Si alloy (AlSi14.510Mg5.630), the exponents in (1) should amount 0.3405 and 0.30. In the alloys from Al-Si-Fe system [32], similar values of c_1 and n_1 were observed. For the AlSi7.837Fe0.521 alloy, in that similarly to current α-Al first (AlSi9.430Mg3.470) alloy α-Al precipitate grows as first, n_1 amounts 0.311 and 0.38 respectively. The values of n_1 gained in current work and in mentioned studies [32-34] for slow solidification generally increased as effect of flow, but are significantly smaller than the values of 0.47–0.50 for directional solidification [43].

In the situation where dendrites are stable mounted in solidified alloy and not moving, the melt flow flowing around the dendrites changes significantly SDAS, and it is confirmed by the coefficients 0.47–0.50 for directional solidification [43]. By slow solidification leading to equiaxed dendrites with possibility of free flow in the melt, the changes in SDAS are smaller but still significant, as marked by currently calculated n_1=0.38 coefficient, and measured SDAS that increased from 54.8 to 68.3 μm.

The comparison of n_1 coefficients may indicate another effect of intermetallic phases arising between the dendrites that has not yet been resolved. The shape and number density, and distribution of Mg_2Si, Mn-intermetallics and β-Al_5FeSi phases in Al-Si-Mg, Al-Si-Mn [33,34] and Al-Si-Fe [32] systems respectively, may differently be modified by flow generated with coils.

The fact that in all studied alloys, the grain size L_{Al} of α-Al phase decreased (Tab. 1), e.g. 66% for α-Al first alloy, support idea that by freely flowing dendrites, SDAS changes are smaller. The decreasing L_{Al} (smaller grains) mean that α-Al phase can be lifted more easily and faster, and therefore the relative movement of the liquid alloy towards arms of α-Al is smaller, reducing λ_{SDAS} weaker.

To characterize the complicated shape of α-Al phase occurring as dendrites or spherical forms, the specific interfacial area S_v was introduced [44] and developed [45] and proposed as a factor dependent on solidification time t:

$$S_V \sim t^{-1/3} \tag{2}$$

where t is in min, and with increasing forced flow in AlCu30 alloy [46], S_V may reach lower values, changing from 0.077 to 0.035 μm^{-1} .

The 31% and 29% forced convection caused reduction in S_v (Table 1), by much lower standard deviation, for the α-Al first and α-Al/Si alloys, is significant, indicating the more compact shape of the α-Al phases. In the Si first alloy, by some occurring α-Al phases, S_V increased. From Fig. 13 may be deduced that it results from the thinner α-Al phase by melt stirring than by natural convection, by similar looking shape of dendrites. The enclosed area of white α-Al seems to be smaller by similar perimeter for stirring. The specific surface S_v as a marker, seems to alarm more precisely to the presence of melt movement than SDAS.

Table 1.
Microstructure parameters measured on inspected micrographs of AlSiMg alloys

Aluminum Alloys	RMF [mT] {Solid. Time [s]}	Dendrites - α-Al phase			Eutectics		
		λ_{SDAS} [μm]	L_{Al} [μm]	S_v [μm^{-1}]	λ_{AlSi} [μm]	$\lambda_{Al\text{-}Mg2Si}$ [μm]	$\lambda_{Ternary}$ [μm]
"α-Al first" alloy AlSi9.430Mg3.470	0{863}	54.8[4.4]	4171[87]	0.0492[0.004]	11.64[0.649]	8.20[2.045]	3.29[0.200]
	11{621}	68.3[3.9] (17%)	1428[52] (-66%)	0.0338[0.002] (-31%)	7.44[0.974] (-36%)	8.31[1.985] (1%)	5.33[0.342] (62%)
"Mg_2Si first" alloy AlSi13.070Mg5.845	0{561}	-	-	-	19.59[2.591]	15.51[2.468]	11.13[1.816]
	11{679}	-	-	-	11.32[1.756] (-42%)	14.04[1.154] (-9%)	5.39[0.428] (-52%)
"Si first" alloy AlSi14.180Mg4.400	0{690}	41.4[8.3]	2556[72]	0.0643[0.005]	8.42[0.575]	7.45[0.379]	3.19[0.178]
	11{521}	43.8[2.2] (6%)	1491[33] (-42%)	0.0797[0.009] (24%)	10.62[1.554] (26%)	6.42[0.510] (-14%)	2.32[0.172] (-27%)
"α-Al/Mg_2Si" alloy AlSi6.470Mg7.840	0{984}	-	-	-	9.41[0.697]	19.02[1.835]	5.24[0.807]
	11{1111}	-	-	-	12.31[0.922] (31%)	21.55[2.691] (13%)	3.98[0.672] (-24%)
"α-Al/Si″ alloy AlSi12.515Mg2.250	0{1133}	67.7[5.7]	4044[119]	0.0428[0.003]	24.97[3.201]	13.18[1.712]	8.26[1.083]
	11{881}	71.0[2.6] (5%)	1627[28] (-60%)	0.0305[0.004] (-29%)	25.39[2.294] (2%)	14.02[1.285] (6%)	6.20[0.680] (-25%)
"Mg_2Si/Si" alloy AlSi14.510Mg5.630	0{567}	38.7[2.9]	1710[75]	0.0768[0.006]	8.92[1.134]	8.02[1.005]	4.08[0.117]
	11{725}	34.8[1.9] (-10%)	1233[63] (-28%)	0.0826[0.009] (8%)	6.68[0.735] (-25%)	8.32[1.445] (4%)	3.43[0.257] (-16%)

(1) Brackets [the standard deviation]; (2) Dash – by absence of phases, lack of data; (3) Curly brackets {the solidification time (s)}; (4) Parentheses (parameters variation [%] resulting from induced by electric coils forced flow).

4.2. Mg-phases

Mg_2Si phase precipitates also in technical alloys with more complex composition, e.g. in AlMgSiFeMn [30], not as simply as currently studied. In contrary to α-Al or AlSi-eutectics, Mg_2Si are a minority, by mass fraction from 0 to about 12%, similarly to previously studied Fe-rich [32,], Mn-rich [33,34,47] phases and in Cu [31] and Mg [30] containing alloys, investigated in directional solidification or by slow cooling like in current work.

Melt flow decreased the dimension L_{Mn} of Mn-rich precipitates by 9% in AlMg5Si5Mn1 alloy [30] and by 19% in the AlCu4Si6Mn2 alloy [31] where $Al_{15}Si_2Mn_4$ solidify as first before AlSi-eutectics and α-Al, by slow cooling. Whilst stirring reduced L_{Mn} by 42% in AlCu4Si6Mn0.65 alloy [31], where Mn-phases start to precipitate by common growth after α-Al. In directionally solidified under forced flow specimens of AlSiMn alloys [47], the pre-eutectic Mn intermetallics grew smaller, whilst inter-eutectic were larger.

For Fe-rich β-Al_5FeSi intermetallics, by intensive stirring, significant 80% decrease in the dimension (length) or complete destruction was observed [48], but the reduction depends on cooling conditions too [49]. In directional solidification of AlSiFe alloys [50,51], by forced flow leading to segregation, increase in β-Al_5FeSi length may also occur, from 160 to 280 μm [50], or by 9% [51]. The flow effect on β-Al_5FeSi, eutectics and α-Al phase may be reduced by the presence of Mg_2Si in AlMgSiFeMn alloys [30] by dumping flow or may be determined by other elements like Cu in AlCu4Si6Fe1 [31] with e.g. 33% reduction in β length

or 76% and 23% increase for AlCu4Si6Fe2 and AlCu10Si10Fe1 alloys [31]. From histograms showing whole intermetallics population is known that stirring causes higher amount of short β-Al_5FeSi [51]. Beside composition, the precipitation sequence of phases may determine flow effect, e.g. when β-Al_5FeSi grow in fully liquid alloy, the length may increase 92% and 76% in AlSi12.795Fe1.705 and AlSi12.911Fe2.372 alloys respectively [32], whilst decrease 14% by presence of α-Al in AlSi7.837Fe0.521 alloy [32]. But by β-Al_5FeSi characterization, the measurement and calculation method should be carefully considered, as e.g. average length, overall dimension, number density or Feret diameter [30-34,51-52].

Table 2.
Microstructure parameters measured on inspected micrographs of "α-Al/Mg_2Si" alloy

Aluminum Alloys	RMF [mT]	Dendrites		
		λ_X [μm]	$\lambda_{X\text{-}Mg2Si}$ [μm]	$\lambda_{X\text{-}Al\text{-}Mg2Si}$ [μm]
"α-Al/Mg_2Si" alloy AlSi9.430Mg3.470	0	62.73 [5.727]	3.90 [0.332]	22.04 [2.255]
	11	69.35 [5.814] (10%)	3.84 [0.328] (-2%)	21.60 [2.079] (-2%)

Table 3.
Microstructure parameters measured on inspected micrographs of "Mg_2Si first" alloy

Aluminum Alloys	RMF [mT]	Dimension L of primary Mg_2Si phases		
		L_{blocky} [μm]	$L_{dispersed}$ [μm]	$L_{Chinese}$ [μm]
"Mg_2Si first" alloy AlSi13.070Mg5.845	0	91.1 [5.975]	62.9 [2.615]	113.8 [3.794]
	11	128.9 [10.584] (41%)	21.8 [0.607] (-65%)	245.9 [9.699] (116%)

Table 4.
Microstructure parameters measured on inspected micrographs of "Mg_2Si first" alloy

Aluminum Alloys	RMF [mT]	Number density n of primary Mg_2Si phases		
		n_{blocky} [mm^{-2}]	$n_{dispersed}$ [mm^{-2}]	$n_{Chinese}$ [mm^{-2}]
"Mg_2Si first" alloy AlSi13.070Mg5.845	0	2.093	510.0	4.189
	11	4.567 (118%)	7.232 (-98%)	18.28 (336%)

Also the amount of intermetallics, characterized by its number density n_{Mn}, may change under flow. Number density n_{Mn} of Mn phases increased 30% by stirring in AlMg5Si5Mn1 alloy [30], whilst decreased 41% in AlCu4Si6Mn2 alloy [31].

Amount of iron-rich phases may also change under flow depending on cooling conditions in AlSi6.8Fe0.8 alloy [49]. The changes in number density n_β of β-Al_5FeSi may be determined in AlMgSiMn alloys by reducing flow Mg_2Si phases [30]. In Al-Cu-Si system [31] with Fe, forced convection by growing as first β-Al_5FeSi decreased n_β, whilst increased in alloys where β started to grow after α-Al phase. Stirring by growth of β platelets in the melt only promotes higher number density n_β, whilst lower n_β in the melt with presence of α-Al phase, in slow solidification [32], similarly to directional solidification [51]. Different effects may cause convection by joint growth of Si crystals and β [32,51].

Analysis of Al-Si-Mn system led to separate consideration of pre-eutectic (average dimension L_{Mn} = 382-616 μm) and inter-eutectic phases (L_{Mn} = 9.98-47.88 μm). In AlSiMn alloys, forced convection caused 13% more inter-eutectic Mn phases by its 44% dimension reduction in Mn-first alloy where also pre-eutectic Mn-phases grow [34]. Opposite effect was observed for pre-eutectic phases, flow caused larger precipitates (6%) by 10% lower amount. In the alloys where Si crystals precipitate first, melt flow led to smaller inter-eutectic Mn-phases.

In the Al-Si-Mn alloy [34] ("Mn-first" with composition AlSi12.546Mn1.011), where Mn-phases grow as first, forced convection caused 6% larger pre-eutectic phases. The stronger melt stirring effect was observed for "Mn/Si" alloy (AlSi14.870Mn1.159) [34], where pre-eutectic Mn and Si crystals grow together starting from liquidus temperature, and convection led to larger Mn phases (61%) by lower number density (68%). Flow determines also the location of various phases across solidified samples. By the absence of α-Al during first stage of solidification [34], in Mn/Si alloy, stirring reduced by 68% number density n_{Mn} from 0.372 to 0.120 mm^{-2} (Table 2, [34]), and in some central placement from 0.084 to 0.0395 mm^{-2}, and generally, centrum of sample stays empty of Mn phases. In Mn-first alloy n_{Mn} reduction amounts only 10 %, but in centrum opposite effect was observed, where n_{Mn} increased from 0.367 to 0.508 mm^{-2}.

Forced flow increased by 41% average overall dimension L_{blocky} (Tab. 3) of blocky shaped Mg_2Si, and increased by 118% its number density n_{blocky} (Tab. 4). Similarly, stirring increased by 116% and by 336%, average overall dimension (Tab. 3) and number density (Tab. 4) of Chinese script shaped Mg_2Si. The opposite situation occurred for small dispersed Mg_2Si precipitates, where forced convection decreased by 65% and by 98%, average overall dimension (Tab. 3) and number density (Tab. 4).

Flow promotes the growth of Chinese script and blocky phases instead of dispersed phases, which apparently after nucleation of the first Mg_2Si have better conditions for growth than without the presence of flow. Therefore more large blocky and Chinese script appear at the expense of dispersed. So the specificity of growth may be similar to Fe-rich β-Al_5FeSi, which in the liquid alloy, in the presence of flow, acquire larger sizes, in contrast to the behavior of Mn-rich phases, which then become smaller. It should also be noted (Figure 11a) that the α-Al phase growing next to the dispersed phases (probably at the end of solidification according to the precipitation sequence - Tab. 5) appears around the Chinese script and blocky phases co-forming them (Fig. 11b). Flow also caused a larger area occupied by the AlSi eutectic precipitates around the Chinese script, blocky and some α-Al.

In Mg_2Si/Si alloy forced flow caused the formation of distinct dendritic Mg_2Si in the outer area of the sample (Fig. 19), probably as a result of enrichment of this area in Mg, instead of less distinct ones as shown in Fig. 18. Similarly, α-Al precipitates appeared (Figs. 20 and 9a) outside the sample, which were more evenly distributed without forced flow (Fig. 9a). The use of flow in the case of the Mg_2Si/Si alloy can cause the formation of phases on the casting surface, which exhibits e.g. high melting temperature (1085 ˚C) and high hardness (4500 $MN \cdot m^{-2}$) [3,4].

Table 5.
Precipitation sequence in studied Al-Si-Mg alloys

Alloy	Reaction	Temperature Range of Reaction	Mass Fraction of Solid Phases [%] (the Rest is Liquid Alloy) at the Temperature [°C]			
			Temperature	α-Al	Mg_2Si	Al-Si Eutectics
"α-Al first" alloy AlSi9.430Mg3.470	L → α-Al + L	585–558.67	558.67	72.38	0.0	0.0
	L → α-Al + Mg_2Si + Si	558.67–558.65	558.65	89.03	4.33	6.64
"Mg_2Si first" alloy AlSi13.070Mg5.845	L → Mg_2Si + L	585–558.67	558.67	0.0	2.30	0.0
	L → α-Al + Mg_2Si + Si	558.67–558.65	558.65	82.88	8.16	8.96
"Si first" alloy AlSi14.180Mg4.400	L → Si + L	585–558.67	558.67	0.0	0.0	1.90
	L → α-Al + Mg_2Si + Si	558.67–558.65	558.65	83.23	5.87	10.90
"α-Al/Mg_2Si" alloy AlSi6.470Mg7.840	L → α-Al + Mg_2Si+ L	585–558.67	558.67	76.80	10.48	0.0
	L → α-Al + Mg_2Si + Si	558.67–558.65	558.65	87.59	11.24	1.17
"α-Al/Si" alloy AlSi12.515Mg2.250	L → α-Al + Si+ L	568–558.67	558.67	52.74	0.0	6.73
	L → α-Al + Mg_2Si + Si	558.67–558.65	558.65	87.13	2.43	10.44
"Mg_2Si/Si" alloy AlSi14.510Mg5.630	L → Mg_2Si + Si + L	585–558.67	558.67	0.0	2.07	1.71
	L → α-Al + Mg_2Si + Si	558.67–558.65	558.65	81.63	7.83	10.54

4.3. Eutectics

The formation of eutectics proceeds according to the mechanism in which two phases grow under diffusion conditions but without the exchange of the solute in the solid state. The solute pushed out of the solid phase moves to the portion of the liquid alloy located close to the solidification front. The concentration of the accumulated solute depends primarily on the distance from the solidification front and also on the mass exchange and dynamics of the front movement [42,43]. Additionally it depends of course on the type of alloy and the concentration of alloying elements in the whole alloy, which was indicated in the case of the AlCuSiFeMn alloy [31] solidifying in slow conditions and with a small temperature gradient. The eutectic spacings are also influenced by the intensity of convective movements, which was proven in the example of the AlSi alloy solidifying directionally in the form of a cylindrical sample with a diameter of 8 mm in an electromagnetic field of strength of 6 mT. The flow rate and thus the eutectic gaps can also be influenced by minor phases, e.g. Mg_2Si in the AlMgSiFeMn alloy [30], which can affect the spacing by reducing the flow.

In α-Al-first alloy [Table 1], the changes in eutectic spacing λ_{AlSi} are -36% whilst 62% in $\lambda_{Ternary}$. The direction of the change is opposite and perhaps flow causes some migration effect between both eutectics. By observed Al-Mg_2Si eutectics spacing stay almost unchanged. In this alloy the majority is α-Al (about 90% of mass fraction) in opposite to eutectics.

In Mg_2Si-first alloy [Table 1], forced convection degreased all eutectic spacings (42%, 9%, 52%) and this effect of structure changes is well seen of Fig. 11 a and b. The tendency to formation larger Chinese script and blocky instead of dispersed Mg_2Si modified probably solute concentration in spaces between Mg-rich phases.

In Si-first alloy [Table 1], electromagnetic stirring increased eutectic spacing λ_{AlSi} (26%), whilst decreased $\lambda_{Al\text{-}Mg2Si}$ (14%) and $\lambda_{Ternary}$ (27%) and by calculated standard deviations, only the last one $\lambda_{Ternary}$ should be considered.

In α-Al/Mg_2Si alloy [Table 1], electromagnetic stirring increased eutectic spacing λ_{AlSi} (31%) and $\lambda_{Al\text{-}Mg2Si}$ (13%), whilst decreased $\lambda_{Ternary}$ (24%). It is very interesting structure of this alloy (Fig 14 a and b), which can be describe as a dendritical structure, where the dendrites are built of Mg_2Si phase, with eutectic like structure. These α-Al/Mg_2Si dendrites behave like dendrites, because flow modified long arms into shorter or to globular forms, typically like in α-Al-first alloy (Fig. 10). So, the general shape of α-Al/Mg_2Si changed under flow as α-Al phase, from dendritic to globular, whilst its lamellar interior responded in another way to flow, by changes -2% and -2% (Table 2) for $\lambda_{X\text{-}Mg2Si}$ and $\lambda_{X\text{-}Al\text{-}Mg2Si}$ that are negligible. The spacing λ_X, similar to secondary dendrite arms spacing of α-Al phase, increased 10% under forced flow. The values of λ_X (62.73 and 69.35 μm) seems

to be similar to secondary dendrite arm spacing λ_{SDAS} (54.8 and 68.3 μm) of α-Al phase in α-Al first alloy (Tab. 1).

In the tested alloys, eutectics are released in the last stage of solidification (Tab. 5), during which the sample is still penetrated by an electromagnetic field that can induce flow and modify the structure. The varied changes in the tested eutectics under the influence of convection are ambiguous and require further research. It seems that both the size, shape of the sample, and the method of solidification should be adapted to the study of only alloys with an eutectic composition, and not as wide as in the present work. The analysis of the effect of convection on eutectics requires a separate approach.

4.4. Solidification by stirring

In the α-Al-first alloy, the α-Al phase precipitated itself from the liquidus temperature (Table 5) to 558.67 °C, and forced convection induced an increase in SDAS by 17% (Table 1), a decrease in specific surface by 31%, 66% reduction in grain size L_{Al}, as well as changes in eutectic spacing. The changes of the α-Al phase from the dendritic form (Fig. 4a, 10a) to the globular one (Fig. 4b, 10b) with single dendrites are consistent with previous investigations [30-34, 16-26], e.g. in the AlSi7.887Mn0.379 alloy [33] the SDAS of the self-precipitating α-Al phase increased by 9% while specific surface decreased by 42%. The study of this alloy align with the previous results [30-34, 16-26]. But by all SDAS determination methods, the calculation model should be carefully considered [42-46, 53-54]. The grain size L_{Al} was also reduced in all other alloys where α-Al was present (α-Al-first, Si-first, α-Al/Si and Mg_2Si/Si alloys).

The Mg_2Si phase precipitated in the Mg_2Si-first alloy independently, and forced flow induced significant changes in the size and density of occurrence. The size of the blocky shaped phases increased (Table 3) by 41% and Chinese script by 116%, while it decreased by 65% for the dispersed phases. The density of occurrence (Table 4) increased by 118% and 336% for the blocky phases and Chinese script, respectively, while it decreased for the dispersed by 98%. Electromagnetic stirring induced a clear change in the structure of this alloy (Fig. 11a), promoting large blocky and Chinese script phases, causing the disappearance of small dispersed Mg_2Si phases and changing the form of the α-Al phase precipitation, which is completely new. In the work [30], Al-Mg-Si alloys were studied, however, in the analyzed alloys, the Mg_2Si phase never grew independently as the first one. In the work [32] a similar effect was demonstrated, where in the β-first (AlSi12.795Fe1.705) and β-2-first (AlSi12.911Fe2.372) alloys, the Fe-rich β-Al_5FeSi phases grew larger under the influence of flow, 92% and 76%, respectively, with a reduced density of occurrence n_β of 71% and 70% (Table 2 in [32]). Mn-rich phases were subjected to solidification under similar conditions [33,34], however, the indications here are ambiguous. Apparently, the Mg-rich phases behave analogously to the Fe-rich phases in free growth conditions. In the tested Mg_2Si-first alloy, the phase precipitating independently (Table 5) in the temperature range from liquidus 585 °C to 558.67 °C reached a mass fraction of 2.30% only. Mg_2Si was freely floating and flowing in an almost completely melt, i.e. their nucleation and growth were not influenced by mechanical interactions, but rather by the temperature field and concentration field determined by convective regime. The clear change in morphology indicates the possibility of significant influence of flow on Mg_2Si.

In the α-Al/Mg_2Si alloy, α-Al and Mg_2Si co-precipitated in the range of 585-558.67 °C (according to monovariant – violet dashed line – Fig. 1) in the amount reaching just before the solidus temperature the mass fraction of 76.80% and 10.48% (Tab. 5), respectively. Basically, a common structure was formed here (Fig. 3) with a basically dendritic shape (like α-Al dendrites) but with a filling in the form similar to Mg_2Si (Fig. 14a), and here the flow increased the dendritic spacing λ_X (Fig. 3) by 10% (Tab. 2, Fig. 14a) and caused partial globular precipitation (Fig. 14b) instead of dendritic (Fig. 14a) and did not change the spacing in the interior (negligible change -2%, Tab. 2). This observation is new and indicates a selective influence of flow on such an α-Al/Mg_2Si structure (Fig. 7, 14). Thus, in technical alloys with a more complex composition than those currently studied, in the presence of segregation, in alloy portions with a chemical composition consistent with the tested α-Al/Mg_2Si alloy, flow can induce changes consistent with the presented pattern (Fig. 14, Tab. 2). In previously studied Al-Mg-Si alloys (e.g. AlMg5Si5Fe1 or AlMg5Si5Mn1) [33], α-Al and Mg_2Si phases precipitated concurrently, but in the presence of other phases (e.g. Fe-rich and Mn-rich phases) and with a small amount of Mg_2Si, a similar effect was not observed. In previous studies, such an effect of flow was not found.

In the α-Al/Si alloy, α-Al and Si crystals precipitated concurrently in the range of 585-558.67 °C (Table 5), and in the amount reaching just before the solidus mass fraction temperature 52.74% and 6.73%, respectively. Flow caused the α-Al phase changes (Figs. 8, 15), SDAS increased by 5% and specific surface S_V decreased by 29% (Table 1) and results are consistent with the previous one [32], where in the α-Al/Si alloy of composition AlSi12.587Fe0.443, SDAS increased by 35% and S_V decreased by 15%, and similarly in the α-Al/Si alloy of composition AlSi12.536Mn0.296 [33] SDAS increased by 14% and S_V decreased by 25%. Characteristic is the appearance of eutectic-enriched areas under the influence of electromagnetic stirring (Fig. 15b), which almost do not occur at all during natural convection (Fig. 15a). This effect is also visible in the view of the entire cross-section of the sample (Fig. 8), where it can be also seen that the flow also caused shorter or smaller dendritic α-Al precipitations (Fig. 8b) and the appearance of globular α-Al (Fig. 15b). The above effect can help in the interpretation of flow conditions in castings, where the observation of eutectic-enriched areas clearly separated from the dendritic zone may suggest turbulent filling of the casting mold.

In the Mg_2Si/Si alloy, Mg_2Si and Si crystals precipitated concurrently in the range of 585-558.67 °C (Table 5), and in the amount reaching just before the solidus temperature the mass fraction of 2.07% and 1.71%, respectively. The precipitated phases could freely float and grow in the almost completely liquid alloy, and apparently mechanical interactions between them did not occur, and their precipitate was determined by the temperature and concentration field dependent on natural or forced convection. In this alloy, convection caused the distinct appearance of Mg_2Si dendrites (Fig. 16b and 19b) in the outer part, on the surface of the sample with the crucible, and similarly, α-Al dendrites (19b and 20) became more distinct in this area,

which are absent at 0 mT (Fig. 16a, 9a) or are less developed (Fig. 18).

4. Conclusions

1. In tested Al-Si-Mg alloys, electromagnetic stirring caused melt flow and led to microstructure modification: changed amount, dimension, and location of magnesium-rich Mg_2Si precipitates, secondary dendrite arm spacing SDAS, specific surface S_v and grain size L_{Al} of α-Al phase (shaped as dendritical or globular), and finally modified eutectic spacing for observed binary and ternary eutectics,
2. The forced flow increased SDAS, decreased S_v and L_{Al}, and caused globular α-Al in α-Al-first alloy (AlSi9.430Mg3.470). The grain size of α-Al was also reduced in other alloys where α-Al was present,
3. In Mg_2Si-first alloy (AlSi13.070Mg5.845) flow produced more and larger blocky shaped and Chinese script phases and significantly reduced amount and dimension of dispersed Mg_2Si,
4. The co-precipitation of α-Al and Mg_2Si (according to monovariant transformation) in AlSi6.470Mg7.840 alloy caused formations with a basically dendritic shape (like α-Al dendrites) but with a filling in the form of Mg_2Si (instead of pure α-Al), and forced flow increased its SDAS, produced globular forms instead of dendritical, whilst did not change the internal spacing,
5. In the α-Al/Si alloy (AlSi12.515Mg2.250), where α-Al and Si crystals co-precipitated concurrently, stirring increased SDAS, decreased specific surface S_v and grain size of α-Al, produced smaller dendrites and globular forms. Convection caused formation of characteristic eutectic-enriched regions separated from α-Al rich regions,
6. In the Mg_2Si/Si alloy (AlSi14.510Mg5.630), convection caused the distinct appearance of dendritic Mg_2Si and some dendritic α-Al in the outer part of the specimen, on the surface between the sample and crucible,
7. The observed structural modifications are new and can help in assessing the effect of convection on the microstructure of industrial Al alloys. The modifications can also support the design of casting processes in which forced convection is the main phenomenon determining the microstructure and properties of cast parts e.g. in rheocasting, mechanical or electromagnetic stirring, melt conditioning (MC) and continuous casting by rotating magnetic field RMF.

Acknowledgements

The research leading to these results has received partial funding from the People Programme (Marie Curie Actions) of the European Union's Seventh Framework Programme (FP7/2007–2013) under the REA grant agreement n° PCIG13-GA-2013-613906. More information on the funded projects is available at: www.iFlowFePhase.info. This research was partially founded by the Ministry of Science and Higher Education in Poland, allocated at Poznan University of Technology, grant number 0613/SBAD/4770.

References

[1] Mondolfo, L.F. (1976). *Aluminium Alloys: Structure and Properties*. Butterworths & Co.: London, UK.
[2] Nong, G. (Eds.). (2018). *Aluminum Alloys*. MDPI. Switzerland.
[3] Lu, L., Lai, M.O. & Hoe, M.L. (1998). Formation of nanocrystalline Mg2Si and Mg2Si dispersion strengthened Mg-Al alloy by mechanical alloying. *Nanostructured Materials*. 10(4), 551-563. https://doi.org/10.1016/S0965-9773(98)00102-0.
[4] Wang, L. & Qin, X.Y. (2003). The effect of mechanical milling on the formation of nanocrystalline Mg_2Si through solid-state reaction. *Scripta Materialia.* 49(3), 243-248. https://doi.org/10.1016/S1359-6462(03)00241-0.
[5] Kim, B.J., Jung, S.S., Hwang, J.H., Park, Y.H. & Lee, Y.C. (2019). Effect of eutectic Mg_2Si phase modification on the mechanical properties of Al-8Zn-6Si-4Mg-2Cu cast alloy. *Metals.* 9, 32, 1-10. https://doi.org/10.3390/met9010032.
[6] Emamy, M., Emami, A.R. & Tavighi, K. (2013). The effect of Cu addition and solution heat treatment on the microstructure, hardness and tensile properties of Al-15%Mg2Si-0.15%Li composite. *Materials Science and Engineering:. A*. 576, 36-44. https://doi.org/10.1016/j.msea.2013.03.066.
[7] Zhang, J., Fan, Z. Wang, Y.Q. & Zhou, B.L. (2000). Microstructural development of Al-15wt.% Mg2Si in situ composite with mischmetal addition. *Materials Science and Engineering: A*. 281(1-2), 104-112. https://doi.org/10.1016/S0921-5093(99)00732-7.
[8] Emamy, M., Khorshidi, R. & Raouf, A.H. (2011). The influence of pure Na on the microstructure and tensile properties of Al-Mg2Si metal matrix composite. *Materials Science and Engineering: A.* 528(13-14), 4337-4342. https://doi.org/10.1016/j.msea.2011.02.010.
[9] Li, C.,Wu, Y., Li, H.,Wu, Y. & Liu, X. (2010). Effect of Ni on eutectic structural evolution in hypereutectic Al-Mg2Si cast alloys. *Materials Science and Engineering: A.* 528(2), 573-577. https://doi.org/10.1016/j.msea.2010.09.056.
[10] Tebib, M., Samuel, A.M., Ajersch, F. & Chen, X.G. (2014). Effect of P and Sr additions on the microstructure of hypereutectic Al-15Si-14Mg-4Cu alloy. *Materials Characterization*. 89, 112-123. https://doi.org/10.1016/j.matchar.2014.01.005.
[11] Qin, Q.D., Zhao, Y.G., Zhou,W. & Cong, P.J. (2007). Effect of phosphorus on microstructure and growth manner of primary Mg2Si crystal in Mg_2Si/Al composite. *Materials Science and Engineering: A.* 447(1-2), 186-191. https://doi.org/10.1016/j.msea.2006.10.076.
[12] Jiang, W., Xu, X., Zhao, Y., Wang, Z., Wu, C., Pan, D. & Meng, Z. (2018). Effect of the addition of Sr modifier in different conditions on microstructure and mechanical properties of T6 treated Al-Mg2Si in-situ composite. *Materials Science and Engineering: A.* 721, 263-273. https://doi.org/10.1016/j.msea.2018.02.100.

[13] Sun, J., Li, C., Liu, X., Yu, L., Li, H. & Liu, Y. (2018). Investigation on AlP as the heterogeneous nucleus of Mg2Si in Al-Mg_2Si alloys by experimental observation and first-principles calculation. *Results in Physics.* 8, 146-152. https://doi.org/10.1016/j.rinp.2017.11.025.
[14] Li, C., Liua, X. & Zhang, G. (2008). Heterogeneous nucleating role of TiB2 or AlP/TiB2 coupled compounds on primary Mg2Si in Al-Mg-Si alloys. *Materials Science and Engineering: A.* 497(1-2), 432-437. https://doi.org/10.1016/j.msea.2008.07.034.
[15] Zhang, Y., Patel, J.B., Lazaro-Nebreda, J. & Fan, Z. (2018). Improved defect control and mechanical property variation in high-pressure die casting of A380 alloy by high shear melt conditioning. *Journal of the Minerals, Metals & Materials Society.* 70, 2726-2730. https://doi.org/10.1007/s11837-018-3005-y.
[16] Das, A., Ji, S., Fan, Z. (2002). Solidification microstructures obtained by a novel twin screw liquidus casting method. In Proceedings of the 7th International Conference on Demi-Solid Processing of Alloys and Composites, 25–27 September (pp. 689–694). Tsukuba, Japan
[17] Sree Manu, K.M., Barekar, N.S., Lazaro-Nebreda, Patel, J.B. & Fan, Z. (2021). In-situ microstructural control of A6082 alloy to modify second phase particles by melt conditioned direct chill (MC-DC) casting process – A novel approach. *Journal of Material Processing Technology.* 295, 117170, 1-14. https://doi.org/10.1016/j.jmatprotec.2021.117170.
[18] Wang, H., Davidson, C.J. & St. John, D.H. (2004). Semisolid microstructural evolution of AlSi7Mg during partial remelting. *Materials Science and Engineering:* A. 368(1-2), 159-167. https://doi.org/10.1016/j.msea.2003.10.305.
[19] Eslami, M., Payandeh, M., Deflorian, F., Jarfors, A.E.W. & Zanella, C. (2018). Effect of segregation and surface condition on corrosion of Rheo-HPDC Al–Si alloys. *Metals*. 8(4), 209, 1-18. https://doi.org/10.3390/met8040209.
[20] Mohammed, M.N., Omar, M.Z., Al-Zubaidi, S., Alhawari, K.S. & Abdelgnei, M.A. (2018). Microstructure and mechanical properties of thixowelded AISI D2 tool steel. *Metals*. 8(5), 316, 1-16. https://doi.org/10.3390/met8050316.
[21] Brollo, G.L., Proni, C.T.W. & Zoqui, E.J. (2018). Thixoforming of an Fe-Rich Al-Si-Cu alloy—thermodynamic characterization, microstructural evolution, and rheological behaviour. *Metals*. 8(5), 332, 1-24. https://doi.org/10.3390/met8050332.
[22] Haga T. & Suziki, S. (2001). Casting of aluminum alloy ingots for thixoforming using a cooling slope. *Journal of Materials Processing Technology.* 118(1-3), 169-172. https://doi.org/10.1016/S0924-0136(01)00888-3.
[23] He, M., Zhang, Z., Mao, W., Li, B., Bai, Y. & Xu, J. (2019). Numerical and experimental study on melt treatment for large-volume 7075 alloy by a modified annular electromagnetic stirring. *Materials*. 12(5), 820, 1-16. https://doi.org/10.3390/ma12050820.
[24] Nakato, H., Oka, M., Itoyama, S., Urata, M., Kawasaki, T., Hashiguchi, K. & Okano, S. (2002). Continuous semi-solid casting process for aluminum alloy billets. *Materials Transactions*. 43(1), 24-29. https://doi.org/10.2320/matertrans.43.24.
[25] Li, Y., Zhou, R., Li, L., Xiao, H. & Jiang, Y. (2018). Microstructure and properties of semi-solid ZCuSn10P1 alloy processed with an enclosed cooling slope channel. *Metals*. 8(4), 275, 1-11. https://doi.org/10.3390/met8040275.
[26] Jiang, J., Xiao, G., Che, C. & Wang, Y. (2018). Microstructure, mechanical properties and wear behavior of the rheoformed 2024 aluminum matrix composite component reinforced by Al_2O nanoparticles. *Metals*. 8(6), 460, 1-24. https://doi.org/10.3390/met8060460.
[27] Modigell, M., Pola, A. & Tocci, M. (2018). Rheological characterization of semi-solid metals: a review. *Metals.* 8(4), 245, 1-23. https://doi.org/10.3390/met8040245.
[28] Flemings, C.M. (1991). Behavior of metal alloys in the semisolid state. *Metallurgical Transactions:* B. 22, 269-293. https://doi.org/10.1007/BF02651227.
[29] Mikolajczak, P., Janiszewski, J., Jackowski, J. (2019). Construction of the facility for aluminium alloys electromagnetic stirring during casting. In Gapiński B., Szostak M., Ivanov V. (Eds.), *Advances in manufacturing II. Vol. 4. Mechanical Engineering* (pp. 164-175). Cham, Switzerland, Springer. https://doi.org/10.1007/978-3-030-16943-5_15.
[30] Mikolajczak, P. (2017). Microstructural evolution in AlMgSi alloys during solidification under electromagnetic stirring. *Metals.* 7(3), 89, 1-16. https://doi.org/10.3390/met7030089.
[31] Mikolajczak, P. (2021). Effect of rotating magnetic field on microstructure in AlCuSi alloys. *Metals*. 11(11), 1804, 1-23. https://doi.org/10.3390/met11111804.
[32] Mikolajczak, P. (2023). Distribution and morphology of α-Al, Si and Fe-Rich phases in Al–Si–Fe alloys under an electromagnetic field. *Materials*. 16(9), 3304, 1-31. https://doi.org/10.3390/ma16093304.
[33] Mikolajczak, P. (2023). Morphology and distribution of α-Al and Mn-rich phases in Al-Si-Mn alloys under an electromagnetic stirring. *Archives of Foundry Engineering*. 23(3), 74-87. DOI: 10.24425/afe.2023.146665.
[34] Mikolajczak, P. (2023). Flow effect on Si crystals and Mn-phases in hypereutectic and eutectic Al-Si-Mn alloys. *Archives of Foundry Engineering*. 23(4), 72-86. DOI: 10.24425/afe.2023.146681.
[35] Thermo-Calc 4.1—Software package from Thermo-Calc Software AB. Stockholm. Sweden. Available online: www.thermocalc.se (accessed on June 10th 2024).
[36] Martinez, R.A. & Flemings, M.C. (2005). Evolution of particle morphology in semisolid processing. *Metallurgical and Materials Transactions A.* 36(8), 2205-2210. https://doi.org/10.1007/s11661-005-0339-1.
[37] Mullis, A. (1999). Growth induced dendritic bending and rosette formation during solidification in a shearing flow. *Acta Materialia.* 47(6), 1783-1789. https://doi.org/10.1016/S1359-6454(99)00052-X.
[38] Li, T., Lin, X. & Huang, W. (2006). Morphological evolution during solidification under stirring. *Acta Materialia.* 54(18), 4815-4824. https://doi.org/10.1016/j.actamat.2006.06.013.
[39] Niroumand, B. & Xia, K. (2000). 3D study of the structure of primary crystals in a rheocast Al-Cu alloy. *Materials Science and Engineering: A*. 283(1-2), 70-75. https://doi.org/10.1016/S0921-5093(00)00619-5.

[40] Birol, Y. (2007). A357 thixoforming feedstock produced by cooling slope casting. *Journal of Materials Processing Technology*. 186(1-3), 94-101. https://doi.org/10.1016/j.jmatprotec.2006.12.021.
[41] Das, A., Ji, S. & Fan, Z. (2002). Morphological development of solidification structures under forced fluid flow: A Monte Carlo simulation. *Acta Materialia.* 50(18), 4571-4585. https://doi.org/10.1016/S1359-6454(02)00305-1.
[42] Stefanescu, D. (2009). *Science and engineering of casting and solidification.* Springer: Boston, MA, USA, ISBN 978-0-387-74609-8. https://doi.org/10.1007/b135947.
[43] Steinbach, S. & Ratke, L. (2007). The influence of fluid flow on the microstructure of directionally solidified AlSi-base alloys. *Metallurgical and Materials Transactions A.* 38, 1388-1394. https://doi.org/10.1007/s11661-007-9162-1.
[44] Marsh, S.P. & Glicksman, M.E. (1996). Overview of geometric effects on coarsening of mushy zones. *Metallurgical and Materials Transactions A.* 27, 557-567. https://doi.org/10.1007/BF02648946.
[45] Loué, W.R. & Suéry, M. (1995). Microstructural evolution during partial remelting of AlSi7Mg alloys. *Materials Science and Engineering:* A. 203(1-2), 1-13. https://doi.org/10.1016/0921-5093(95)09861-5.
[46] Kasperovich, G., Genau, A., & Ratke, L. (2011). Mushy zone coarsening in an AlCu30 alloy accelerated by a rotating magnetic field. *Metallurgical and Materials Transactions A.* 42, 1657-1666. https://doi.org/10.1007/s11661-010-0542-6.
[47] Mikołajczak, P. & Ratke, L. (2014). Three dimensional morphology of Mn-rich intermetallics in AlSi alloys investigated with X-ray tomography. Materials Science Forum, 790–791, 335–340. https://doi.org/10.4028/www.scientific.net/MSF.790-791.335.
[48] Fang, X., Shao, G., Liu, Y.Q. & Fan. Z. (2007). Effects of intensive forced melt convection on the mechanical properties of Fe containing Al-Si based alloys. *Materials Science and Engineering: A.* 445-446, 65-72. https://doi.org/10.1016/j.msea.2006.09.038.
[49] Nafisi, S., Emad, D., Shehata, T. & Ghomashchi, R. (2006). Effects of electromagnetic stirring and superheat on the microstructural characteristics of Al-Si-Fe alloy. *Materials Science and Engineering: A.* 432(1-2), 71-83. https://doi.org/10.1016/j.msea.2006.05.076.
[50] Steinbach, S., Euskirchen, N., Witusiewicz, V., Sturz, L. & Ratke, L. (2007). Fluid flow effects on intermetallic phases in Al-cast alloys. *Transactions of Indian Institute of Metals*. 60(2), 137-141.
[51] Mikolajczak, P. & Ratke, L. (2013). Effect of stirring induced by rotating magnetic field on β-Al5FeSi intermetallic phases during directional solidification in AlSi alloys. *International Journal of Cast Metals Research.* 26(6), 339-353. https://doi.org/10.1179/1743133613Y.0000000069.
[52] Zimmermann G., Theofilatos A., Steinbach S., Viardin A., Sturz L. & Kargl. F. (2025). The influence od convection and iron content on the solidification microstructure of technical aluminum alloys. *Journal of the Minerals, Metals & Materials Society*. 77, 6050-6060. https://doi.org/10.1007/s11837-025-07361-8.
[53] Roósz A., Rónaföldi A., Svéda M. & Veres Z. (2022). Comparison of dynamical and empirical simulation methods of secondary dendrite arm coarsening. *Crystals*. 12(12), 1834, 1-19. https://doi.org/10.3390/cryst12121834.
[54] Mikolajczak, P. (2025). Assessment of thermal conditions by slow solidification in al alloys and the facility. *Archives of Foundry Engineering*. 25(2), 5-20. DOI: 10.24425/afe.2025.153788.